슬래브 하부 수평저항을 고려한 지반위의 콘크리트 슬래브 해석 모델 및 온도하중에 의한 거동 분석

Analysis Models of Concrete Slabs-on-Grade Considering Horizontal Resistance at Slab Bottom and Behavior under Thermal Loads

김 성 민† 안 주 옥*
Kim, Seong Min An, Zu Og
(논문접수일 : 2005년 9월 12일 ; 심사종료일 : 2006년 8월 28일)

요 지

지반위에 놓인 콘크리트 슬래브가 온도하중을 받을 때 지반의 전단저항과 슬래브 하부와 지반과의 마찰 등에 의해 생기는 슬래브 하부의 수평저항을 고려하여 지반위에 놓인 콘크리트 슬래브의 거동을 분석하였다. 지반위의 콘크리트 슬래브와 강성도로포장의 해석에 널리 사용되는 탄성지반위의 얇은 판을 이용하여 슬래브 하부의 수평저항을 고려하기 위한 해석 공식을 유도하였다. 이를 이용하여 판요소와 쉘요소를 이용한 유한요소법에 의한 모델을 개발하여 수치해석 결과를 도출하였다. 해석 공식과 수치해석 모델을 이용한 해석 결과를 비교 분석하였고 매우 비슷한 결과가 도출 되는 것을 알 수 있었다. 슬래브의 상부와 하부에 온도 차이가 있을 때와 슬래브의 온도가 전체적으로 감소할 때, 콘크리트 슬래브의 응력 분포에 슬래브 하부의 수평저항이 미치는 민감성을 여러 가지의 다른 슬래브의 두께, 탄성계수, 그리고 지반의 수직탄성계수 등을 고려하여 분석하였다. 해석 결과에서 온도하중을 받을 때 슬래브 하부의 수평저항은 슬래브의 응력에 매우 큰 영향을 미칠 수 있다는 것을 발견하였다.

핵심용어 : 지반위의 슬래브, 수평저항, 판, 온도, 유한요소

Abstract

The behavior of the concrete slabs on grade considering the horizontal resistance at the slab bottom, which exists due to the shear resistance of the foundation and the friction between the slab and the foundation, has been investigated when the slabs-on-grade are subjected to the thermal load. Analytical formulations have been developed to include the effect of the horizontal resistance at the slab bottom employing the thin plate on an elastic foundation that is widely used for the analysis of concrete slabs-on-grade and rigid pavement systems. Finite element formulations have then been developed using the plate bending elements and the flat shell elements. The solutions from the analytical and numerical models have been compared and showed very good agreement. The sensitivity of the horizontal resistance to the stresses of the concrete slab has been investigated with various values of the slab thickness, elastic modulus, and vertical stiffness of the foundation when subjected to the temperature gradient between the top and bottom of the slab and the uniform temperature drop throughout the slab depth. The analysis results show that the horizontal resistance at the plate bottom can significantly affect the stresses of the slab when the thermal loads are applied.

Keywords *: slab-on-grade, horizontal resistance, plate, temperature, finite element*

1. Introduction

To analyze the behavior of Portland cement concrete(PCC) slabs on grade including PCC pavement systems analytically and numerically, a number of studies have been performed by employing the plate on an elastic foundation(Westergaard, 1925; Tabatabaie, *et al.*, 1980; Huang, 1993; Kim, *et al.*, 1997; Liu *et al.*, 2000; Kim *et al.*, 2002). The PCC slab is analyzed based on the Kirchhoff thin plate theory and the underlying layers are modeled using an elastic foundation, normally a Winkler type foundation. Accordingly, the resistance considered at the slab bottom is the vertical stiffness of the founda-

† 책임저자. 정회원 · 경희대학교 토목건축대학 조교수
전화: 031-201-3795 ; Fax: 031-202-8854
E-mail: seongmin@khu.ac.kr
* 정회원 · 경희대학교 토목건축대학 교수

• 이 논문에 대한 토론을 2006년 12월 31일까지 본 학회에 보내주시면 2007년 3월호에 그 결과를 게재하겠습니다.

tion(modulus of subgrade reaction) and the horizontal resistance at the slab bottom is normally ignored(Kim, *et al.*, 1998; Huang, *et al.*, 2001). However, the shear resistance of the foundation and the friction between the slab bottom and the foundation cause the horizontal resistance applied to the bottom of the slab. If the slab and the foundation are perfectly bonded, the horizontal resistance at the slab bottom will be the same as the shear resistance of the foundation. Even if the slab and the foundation are perfectly debonded, the interface friction will still cause the horizontal resistance at the slab bottom. The horizontal resistance exerts its effect when there are horizontal strains at the slab bottom, which is common with most types of the loads including vertical load, moment, surface traction, temperature gradient, and temperature drop and increase.

The horizontal resistance at the slab bottom can simply be considered by attaching horizontal springs at the slab bottom when the slab is modeled using three dimensional(3D) solid finite elements(Kim *et al.*, 2000). However, computation run time and needed memory to obtain the analysis results are significantly larger for the 3D analysis than those for the analysis based on the plate theory. When the plate on an elastic foundation is analyzed using the plate bending or shell finite elements, the horizontal resistance at the plate bottom cannot be considered directly by attaching the horizontal springs to the degrees of freedom of the finite elements because the degrees of freedom considered in the plate bending or shell elements are assumed to exist at the middle surface of the plate.

In this paper, the methods to include the horizontal resistance at the slab bottom are presented when considering the thin plate theory. In the first part of the paper, the analytical formulations are derived first and the numerical formulations to include the horizontal resistance at the slab bottom are explained when using the plate bending finite elements. The analytical and numerical analysis results are compared and the effects of the horizontal resistance on the stresses are investigated when the PCC slabs on grade are subjected to a temperature gradient between the top and bottom of the slab. In the second part of the paper, the numerical formulations to include the horizontal resistance at the slab bottom are presented when using the shell elements containing five degrees of freedom at each finite element node. Then, the analysis results are compared with those from a more rigorous 3D model. The effects of the horizontal resistance at the plate bottom are investigated when the system is subjected to a temperature drop as well as a temperature gradient. Finally, the findings from this study are summarized.

2. Analytical Formulations Including Plate Bottom Horizontal Resistance

If a plate on a Winkler foundation has horizontal resistance at the bottom of the plate, as shown in Fig. 1, the horizontal resistance will cause internal horizontal forces to the plate bottom when the plate is subjected to external loads. In a Cartesian coordinate system $\{x, y, z\}$, if a horizontal force at the plate bottom in the x direction per unit length in the y direction is $f(x, y)$, the variation of the horizontal force in the x direction in a small segment dx of the plate is

$$\frac{\partial f(x,y)}{\partial x}dx \tag{1}$$

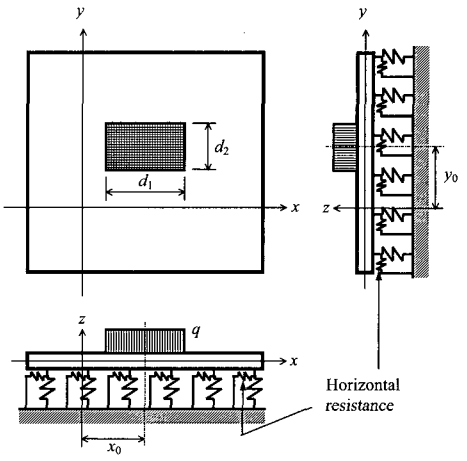

Fig. 1 Plate on Winkler foundation with horizontal resistance at plate bottom.

This horizontal force variation at the plate bottom causes a bending moment with respect to the middle(neutral) surface of the plate and the moment can be calculated by

$$\frac{\partial f(x,y)}{\partial x} dx \frac{h}{2} \tag{2}$$

where h is the thickness of the plate. If the Kirchhoff thin plate theory is considered, equilibrium of the moments around the y axis can be obtained by (Szilard, 2004)

$$\frac{\partial m_x(x,y)}{\partial x} + \frac{\partial m_{yx}(x,y)}{\partial y} - \frac{\partial f(x,y)}{\partial x}\frac{h}{2} = s_x(x,y) \tag{3}$$

where $m_x(x, y)$ and $m_{yx}(x, y)$ are the bending and twisting moments, respectively, per unit length around the y axis, and $s_x(x, y)$ is the transverse shear force per unit length in the x direction. If the horizontal resistance (stiffness per unit area) at the plate bottom is k_h, the force differential $\partial f(x,y)/\partial x$ can be rewritten as

$$\frac{\partial f(x,y)}{\partial x} = -k_h \frac{h}{2}\frac{\partial w(x,y)}{\partial x} \tag{4}$$

where $w(x, y)$ is the vertical displacement. After considering equilibrium of the moments around the x axis similarly, Eq. (5) can be obtained by inserting the moment equilibrium equations into the equilibrium equation of the forces in the z direction.

$$\frac{\partial^2 m_x(x,y)}{\partial x^2} + 2\frac{\partial^2 m_{xy}(x,y)}{\partial x\,\partial y} + \frac{\partial^2 m_y(x,y)}{\partial y^2} + \frac{h^2 k_h}{4}\left(\frac{\partial^2 w(x,y)}{\partial x^2} + \frac{\partial^2 w(x,y)}{\partial y^2}\right) - k w_v(x,y) = -q(x,y) \tag{5}$$

where $m_y(x, y)$ is the bending moment per unit length around the x axis; $m_{xy}(x, y)$ is the twisting moment per unit length around the x axis, which is the same as $m_{yx}(x, y)$; k_v is the vertical stiffness of the foundation per unit area; and $q(x, y)$ is the external vertical force per unit area. By expressing the internal moments m_x, m_y, and m_{xy} in Eq. (5) in terms of the vertical displacement $w(x, y)$, the governing differential equation can be obtained by

$$D_P\left(\frac{\partial^4 w(x,y)}{\partial x^4} + 2\frac{\partial^4 w(x,y)}{\partial x^2\partial y^2} + \frac{\partial^4 w(x,y)}{\partial y^4}\right) - \frac{h^2 k_h}{4}\left(\frac{\partial^2 w(x,y)}{\partial x^2} + \frac{\partial^2 w(x,y)}{\partial y^2}\right) + k_v w(x,y) = q(x,y) \tag{6}$$

where D_P is the flexural rigidity of the plate defined by

$$D_P = \frac{Eh^3}{12(1-\nu^2)} \tag{7}$$

and E and ν are the elastic modulus and Poisson's ratio of the plate, respectively.

3. Finite Element Modeling Including Plate Bottom Horizontal Resistance

As explained with Eqs (1) through (4), the horizontal resistance at the plate bottom can be transferred to the rotational resistance at the neutral surface of the plate with the rotational stiffness per unit area of

$$\frac{h^2 k_h}{4} \tag{8}$$

This rotational resistance can be modeled using rotational springs around the x and y axes. The rotational stiffness K_R at each finite element node can be obtained multiplying the rotational stiffness per unit area in Eq. (8) by the effective area around the node.

$$K_R = \frac{h^2 k_h}{4} \bullet (\textit{Effective area}) \tag{9}$$

If a 4 noded linear plate bending finite element is considered(Fig. 2), the effective area at each node is a quarter of the element area.

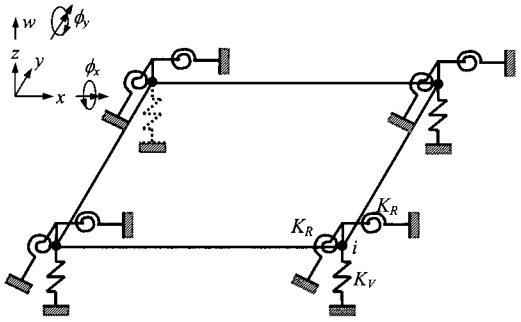

Fig. 2 Plate element with rotational springs.

If the Kirchhoff thin plate theory is applied, each finite element node has three degrees of freedom, which are a displacement in the z direction and rotational displacements around the x and y axes. The equilibrium equation at finite element node i shown in Fig. 2 can then be written as

$$\{F_i\}=\left(\begin{bmatrix}\textit{Stiffness matrix of}\\ \textit{plate bending}\\ \textit{relative to node } i\end{bmatrix}+\begin{bmatrix}K_V & 0 & 0 & 0 & \cdots & 0\\ 0 & K_R & 0 & 0 & \cdots & 0\\ 0 & 0 & K_R & 0 & \cdots & 0\end{bmatrix}\right)\begin{Bmatrix}w_i\\ \phi_{xi}\\ \phi_{yi}\\ \vdots\end{Bmatrix} \tag{10}$$

where F_i are the forces at node i, w_i is the vertical displacement at node i, and ϕ_{xi} and ϕ_{yi} are the rotational displacements around the x and y axes, respectively, at node i. The vertical stiffness of the foundation K_V can be obtained multiplying the vertical stiffness of the foundation per unit area k_v by the effective area.

4. Comparison between Analytical and Numerical Analysis Results

The analytical and the numerical analysis results were compared when a distributed load was applied. To obtain the analytical solution of Eq. (6), the Fourier transform can be used if the plate is assumed to extend to infinity in the horizontal plane. If ξ and ζ are assumed to be the transformed fields of x and y and if $w(x, y)$ and $q(x, y)$ are written in the form of $W(\xi, \zeta)e^{i\xi x}e^{i\zeta y}$ and $Q(\xi, \zeta)e^{i\xi x}e^{i\zeta y}$, the transformed displacement $W(\xi, \zeta)$ can be obtained by

$$W(\xi,\zeta)=\frac{Q(\xi,\zeta)}{D_P(\xi^2+\zeta^2)^2+\frac{h^2k_h}{4}(\xi^2+\zeta^2)+k_v} \tag{11}$$

where the transformed load $Q(\xi, \zeta)$ is obtained using the double Fourier transform

$$Q(\xi,\ \zeta)=\int_{-\infty}^{\infty}\int_{-\infty}^{\infty}q(x,\ y)e^{-i\xi x}e^{-i\zeta y}\,dxdy \tag{12}$$

Then, the vertical displacements can be obtained using the double inverse Fourier transform

$$w(x,y)=\frac{1}{(2\pi)^2}\int_{\infty}^{\infty}\int_{\infty}^{\infty}\frac{Q(\xi,\zeta)}{D_P(\xi^2+\zeta^2)^2+\frac{h^2k_h}{4}(\xi^2+\zeta^2)+k_v}e^{i\xi x}e^{i\zeta y}d\xi d\zeta \tag{13}$$

Finally, the stresses in the x and y directions can be obtained by

$$\sigma_x(x,y,z)=-\frac{Ez}{1-\nu^2}\left(\frac{\partial^2 w}{\partial\eta^2}+\nu\frac{\partial^2 w}{\partial y^2}\right)$$

$$=\frac{Ez}{(1-\nu^2)(2\pi)^2}\int_{\infty}^{\infty}\int_{\infty}^{\infty}\frac{(\xi^2+\nu\zeta^2)Q(\xi,\zeta)}{D_P(\xi^2+\zeta^2)^2+\frac{h^2k_h}{4}(\xi^2+\zeta^2)+k_v}e^{i\xi x}e^{i\zeta y}d\xi d\zeta \tag{14}$$

$$\sigma_y(x,y,z)=-\frac{Ez}{1-\nu^2}\left(\frac{\partial^2 w}{\partial y^2}+\nu\frac{\partial^2 w}{\partial x^2}\right)$$

$$=\frac{Ez}{(1-\nu^2)(2\pi)^2}\int_{\infty}^{\infty}\int_{\infty}^{\infty}\frac{(\nu\xi^2+\zeta^2)Q(\xi,\zeta)}{D_P(\xi^2+\zeta^2)^2+\frac{h^2k_h}{4}(\xi^2+\zeta^2)+k_v}e^{i\xi x}e^{i\zeta y}d\xi d\zeta \tag{15}$$

In practice, the above equations are solved using the Fast Fourier Transform(FFT), which is a discrete transform.

If the model shown in Fig. 1 is used and the load pressure(load per unit area) is q, the transformed load Q defined in Eq. (12) can be obtained by

$$Q(\xi,\zeta)=4q\frac{\sin\frac{d_1\xi}{2}\sin\frac{d_2\zeta}{2}}{\xi\zeta}e^{-i\xi x_0}e^{-i\zeta y_0} \tag{16}$$

where d_1 and d_2 are the loaded lengths of a distributed load in the x and y directions, respectively, and x_0 and y_0 are the coordinates of the center of the load.

The stresses at the bottom of the plate predicted by the analytical and finite element methods are compared first when a distributed load is applied on an infinitely large plate on a Winkler foundation. The properties of the plate on a Winkler foundation and the applied loads used in this study are listed in Table 1. For the FFT in the spaces and the transformed field domains of the spaces, the number of transformed points of 2048 and the distance increment of 1.27cm(0.5in.) were used. For the finite element model, the square plate elements with a length of each element of 5.08cm(2in.) were used. To model the infinite extent of the plate in the horizontal direction and to eliminate the effect of the boundary conditions, the stresses near the load, which were not affected by the size of the plate, were considered to compare with those obtained by the analytical method. The solutions of the finite element model were obtained using a finite element computer program, ABAQUS(ABAQUS, 1998). Note that the stresses at the top and bottom of the plate have the same magnitude with opposite signs.

Table 1 Properties of the plate on a Winkler foundation and applied loads

Plate Properties	
E	27,560MPa (4,000ksi)
v	0.15
k_v	108.8MN/m^3 (400pci)
h	304.8mm (12in.)
Thermal expansion coefficient	0.0000108/°C (0.000006/°F)
Load Properties	
Total load	44.4kN (10kip)
d_1 and d_2	304.8mm (12in.)
Temperature gradient	0.022 °C/mm (1.0°F/in.)

Fig. 3 shows the stresses at the plate bottom from the center of the load along the x direction for various values of the horizontal stiffness at the plate bottom. Fig. 3(a) shows the stresses when there is no horizontal stiffness at the plate bottom. Excellent agreement can be observed between the analytical and finite element analysis results. When there is the horizontal resistance at the plate bottom, as shown in Fig. 3(b) (k_h=408MN/m^3 (1,500pci)) and Fig. 3(c) (k_h=4,080MN/m^3 (15,000pci)), the analysis results between the analytical and numerical methods also show very good agreement. It should be noted that this comparison was made to examine whether the formulations including the horizontal resistance at the plate bottom were correct both in the analytical and the numerical analyses. Since the same results from the analytical and the numerical methods were achieved for the stress distribution due to bending of the plate under a distributed load, the stress distribution due to bending of the plate under a temperature gradient obtained using both methods should be the same.

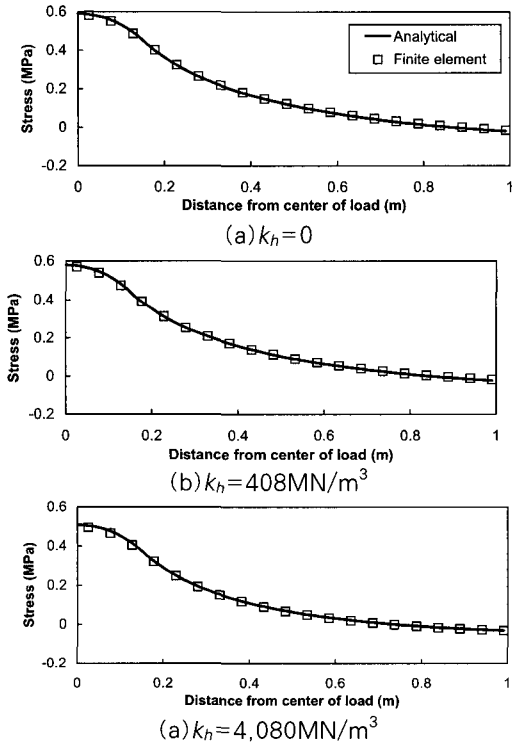

Fig. 3 Comparison between analytical and numerical analysis results.

5. Horizontal Resistance Effects Obtained with Plate Bending Finite Element Model

The effect of the horizontal resistance at the plate bottom on the maximum stress when the temperature gradient is applied is investigated. The temperature gradient considered in this study makes the upper part of the plate contract and the lower part of the plate expand. The plate, therefore, is in the curl up position. Since the foundation resists curling of the plate, the compressive stresses occur at the lower part of the plate and the tensile stresses occur at the upper part of the plate. The length and width of the plate used in this study are 6.096m(20ft) and 3.658m(12ft), respectively, which are the typical dimensions of the jointed concrete pavements. The size of each finite element is 7.62cm (3in.) by 7.62cm(3in.). As shown in Fig. 4, the maximum stress increases as the horizontal stiffness at the plate bottom increases. When the temperature gradient is applied, the vertical resistance of the foundation resists curling of the plate as explained and the stresses occur in the plate. The horizontal resistance at the plate bottom also resists curling of the plate. Therefore, higher stresses are observed as the horizontal stiffness at the plate bottom increases.

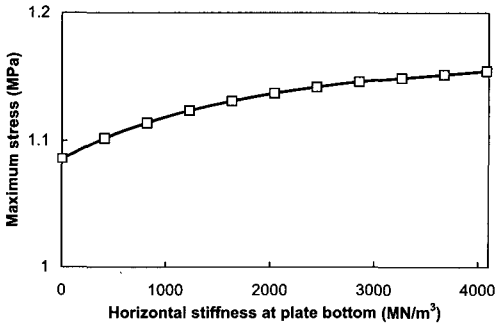

Fig. 4 Effect of horizontal resistance at plate bottom on maximum stress with temperature gradient obtained using plate bending finite elements.

The differences in the maximum stresses of the plates on a Winkler foundation with and without the horizontal resistance at the plate bottom are investigated when the plate is subjected to the temperature gradient and when the plate thickness, plate elastic modulus, and vertical stiffness of the foundation vary. The values of the plate thickness, plate elastic modulus, and vertical stiffness of the foundation considered in this study are within the practical ranges of those for concrete pavement systems(Kim *et al.*, 2003). Fig. 5(a) shows the percent ratio of the maximum stresses obtained with considering the horizontal resistance at the plate bottom to those obtained without considering the horizontal resistance when the thickness of the plate varies. The stress ratio smaller than 100% means that the stress obtained with considering the horizontal resistance is smaller than those obtained without considering it, and the stress ratio larger than 100% means the opposite. The values of the horizontal resistance at the plate bottom of 1,632 and 3,264MN/m^3(6,000 and 12,000pci) were considered. The stress ratio tends to increase as the plate thickness increases. When the plate thickness is larger than about 250 mm, the maximum stresses obtained with considering the horizontal resistance become much larger than those obtained without considering the horizontal resistance at the plate bottom. When the plate thickness is smaller than about 250mm, the reverse occurs but the differences in the maximum stresses obtained with and without considering the horizontal resistance at the plate bottom are not significant. Fig. 5(b) shows the effect of the vertical stiffness of the foundation on the stress ratio. The stress ratio decreases as the vertical stiffness of the foundation increases. When the vertical stiffness of the foundation is smaller than about 200MN/m^3, the maximum stresses obtained with considering the horizontal resistance are larger than those obtained without considering the horizontal resistance, and the differences in the maximum stresses obtained with and without considering the horizontal resistance at the plate

bottom increases significantly as the vertical stiffness of the foundation decreases. When the vertical stiffness of the foundation is larger than about 200MN/m^3, the stress ratio is smaller than but close to 100%. The effect of the elastic modulus of the plate on the stress ratio is shown in Fig. 5(c). The stress ratio increases with increasing the elastic modulus of the plate. The maximum stresses obtained with considering the horizontal resistance are larger than those obtained without considering the horizontal resistance when the elastic modulus of the plate is larger than about 17GPa. Within the ranges of the variables considered in this study, the effect of the horizontal resistance at the plate bottom on the stresses, when the plate is subjected to the temperature gradient, is significant with thicker plate, softer foundation, and larger elastic modulus of the plate.

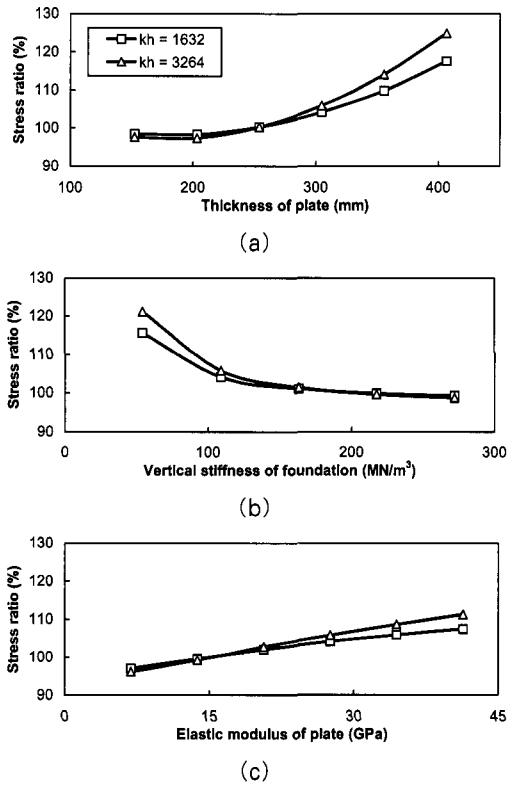

Fig. 5 Differences in stresses obtained with and without considering horizontal resistance when applying a temperature gradient for various values of: (a) plate thickness, (b) vertical stiffness of foundation, (c) plate elastic modulus (unit of kh = MN/m^3).

6. Numerical Modeling Considering In Plane Horizontal Deformations

The formulations explained in the previous sections ignore in plane horizontal deformations at the middle surface of the plate. More rigorous modeling of the plate on a Winkler foundation considering horizontal resistance at the plate bottom is to include horizontal axial deformations of the plate because the horizontal resistance at the plate bottom resists horizontal deformations of the plate as well as bending and curling of the plate. If the horizontal deformations are considered, the responses of the plate caused by horizontal axial loads such as a uniform temperature drop through the depth of the plate can also be obtained.

The in plane horizontal deformations of the plate can be considered by adding two perpendicular horizontal degrees of freedom at each finite element node to the degrees of freedom in the plate bending element that has three degrees of freedom at each node as described previously. Then, the plate element has five degrees of freedom at each node and this element is often called a flat shell element.

If transverse shear deformations are neglected as in the thin plate theory, the straight lines that are initially normal to the middle surface of the plate remain straight and normal to the deflected middle surface. Accordingly, the effect of the horizontal resistance at the plate bottom can be considered with the shell elements by employing rigid beams as shown in Fig. 6(a). The degrees of freedom at node i and at the bottom of the plate(or bottom of the rigid beam) where the bottom resistance exists are shown in Fig. 6(b). Based on the assumptions in the thin plate theory, the vertical and rotational displacements at the middle surface and at the bottom of the plate are the same.

$$w = w_b, \quad \phi_x = \phi_{xb}, \quad \phi_y = \phi_{yb} \tag{17}$$

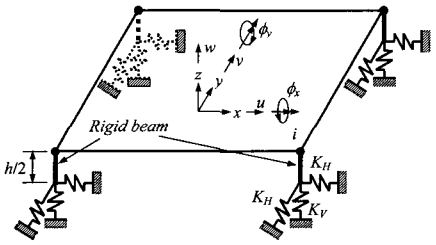

(a) Flat shell element with horizontal springs and rigid beams.

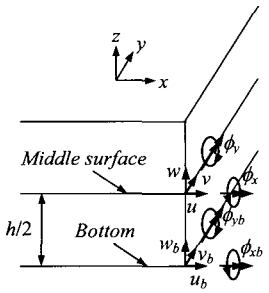

(b) Degrees of freedom.

Fig. 6 Modeling considering in plane deformations.

The horizontal displacements u_b and v_b at the bottom of the plate can be obtained using the displacements at the middle surface by

$$u_b = u - \frac{h}{2}\phi_y, \quad v_b = v + \frac{h}{2}\phi_x \tag{18}$$

where u and v are the displacements in the x and y directions at the middle surface, respectively, and ϕ_x and ϕ_y are the rotational displacements around the x and y axes, respectively. Then, the internal forces and moments created by the horizontal resistance at the plate bottom can be written as

$$F_x = K_H u_b = K_H u - \frac{h}{2}K_H\phi_y \tag{19a}$$

$$F_y = K_H v_b = K_H v + \frac{h}{2}K_H\phi_x \tag{19b}$$

$$M_x = K_H v_b \frac{h}{2} = \frac{h}{2}K_H v + \frac{h^2}{4}K_H\phi_x = \frac{h}{2}K_H v + K_R\phi_x \tag{19c}$$

$$M_y = -K_H u_b \frac{h}{2} = -\frac{h}{2}K_H u + \frac{h^2}{4}K_H\phi_y = -\frac{h}{2}K_H u + K_R\phi_y \tag{19d}$$

where F_x and F_y are the forces in the x and y directions, respectively, and M_x and M_y are the moments around the x and y axes, respectively. The horizontal stiffness K_H can be obtained multiplying the horizontal stiffness per unit area k_h by the effective area. Finally, the equilibrium equation at finite element node i (Fig. 6(a)) can be expressed as

$$\{F_i\} = \left(\begin{bmatrix} \textit{Stiffness matrix of} \\ \textit{flat shell} \\ \textit{relative to node i} \end{bmatrix} + \begin{bmatrix} K_H & 0 & 0 & 0 & -\frac{h}{2}K_H & 0 & \cdots & 0 \\ 0 & K_H & 0 & \frac{h}{2}K_H & 0 & 0 & \cdots & 0 \\ 0 & 0 & K_V & 0 & 0 & 0 & \cdots & 0 \\ 0 & \frac{h}{2}K_H & 0 & K_R & 0 & 0 & \cdots & 0 \\ -\frac{h}{2}K_H & 0 & 0 & 0 & K_R & 0 & \cdots & 0 \end{bmatrix} \right) \begin{Bmatrix} u_i \\ v_i \\ w_i \\ \phi_{xi} \\ \phi_{yi} \\ \vdots \end{Bmatrix} \tag{20}$$

7. Comparison among Different Models

To verify the finite element model developed using the shell elements explained in the previous section, a more rigorous 3D finite element model was also developed using 3D solid elements. The size of a shell element was 7.62cm(3in.) by 7.62cm(3in.) and the size of a 3D solid element was 7.62cm(3in.) by 7.62cm(3in.) in the horizontal plane and 3.81cm(1.5in.) in the vertical direction. Therefore, the number of elements in the vertical direction for the 3D model was 8 to discretize a 12inch thick plate. The horizontal stiffness at the plate bottom was assumed to be 1,632MN/m^3 (6,000pci).

The stresses at the surface and bottom of the plate along the centerline in the x direction from three different models are shown in Fig. 7. The three different models include: (1) a model developed using the plate bending elements that have three degrees of freedom at each finite element node; (2) a model developed using the shell elements that have five degrees of freedom at each finite element node; and (3) a model developed using the 3D solid elements. As shown in Fig. 7, the results from the model developed using the shell elements and the 3D model are in excellent agreement. When the temperature gradient, which

makes the plate in the curl up position, is applied, the models developed using the shell elements and the 3D solid elements yield slightly larger compressive stresses at the bottom of the plate and slightly smaller tensile stresses at the top of the plate compared with the results from the model developed using the plate bending elements. This happens because the horizontal resistance at the plate bottom resists the expansion of the bottom surface of the plate caused by curling of the plate, and as a result, additional horizontal compressive stresses occur over the plate thickness. Since the model developed using the plate bending elements does not include the horizontal degrees of freedom, it cannot consider those additional stresses and the magnitudes of the stresses at the top and bottom of the plate are always the same with this model. In other words, the neutral surface where the stresses in the horizontal plane are zero is always the middle surface of the plate. On the other hand, in the models developed using the shell elements and the 3D solid elements, the neutral surface does not always remain at the middle surface and varies because of the additional horizontal stresses caused by the horizontal resistance at the plate bottom.

Figure 8 shows the stresses at the top and bottom of the plate obtained using the shell elements and the 3D solid elements when a uniform temperature drop is 11.11°C (20°F) over the plate from the reference(zero stress) temperature. The stresses obtained from the two models are basically the same. Since the model consisting of the shell elements needs much smaller computation time and memory compared with the 3D analysis, it is very useful for practical purposes. For instance, when the element sizes of the shell and 3D solid elements in the horizontal plane are the same and if the number of elements in the vertical direction for the 3D solid elements is n, the models with shell and 3D elements need 5 and $3n$ degrees of freedom, respectively, to model the same point with the same slab thickness. This means that if the number of elements is 10 in the vertical direction for the 3D solid elements, the number of degrees of freedom is 33, which is much greater than 5 for the shell elements.

The stresses at the bottom of the plate are larger than those at the top of the plate. Although there is only a horizontal axial load such as a temperature drop, the stresses through the plate thickness are different. This happens because the horizontal resistance at the plate bottom produces the bending(curling) stresses in addition to the horizontal axial stresses. The results from this study show inadequacy of the assumption that the stresses of the plate caused by the friction between the plate and foundation with a temperature drop are constant through the plate thickness(Huang, 1993), which is normally em-

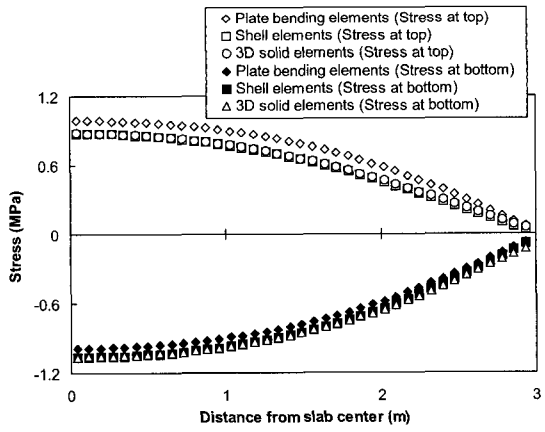

Fig. 7 Comparison between plates with and without considering in plane deformations with temperature gradient.

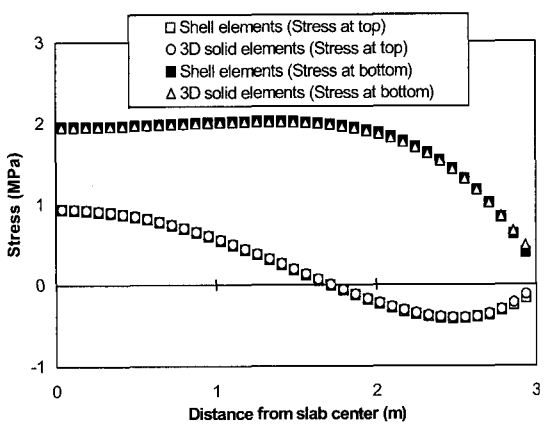

Fig. 8 Comparison with 3D model when a uniform temperature drop is applied.

ployed in the analysis of concrete pavements.

8. Horizontal Resistance Effects with Temperature Gradient

The effects of the horizontal resistance at the plate bottom on the stresses obtained with the model developed using the shell elements are very similar to the previous results obtained with the model developed using the plate bending elements, when the temperature gradient is applied. For instance, Fig. 9 shows the stress ratios between the plates on a Winkler foundation with and without considering the horizontal resistance, when the temperature gradient is applied. As investigated previously with the model developed using the plate bending elements, the stress ratio decreases as the vertical stiffness of the foundation increases. The stress ratios obtained using the plate bending elements lie between the stress ratios at the top and bottom of the plate obtained using the shell elements. The tensile stresses occurred at the top of the plate are close to those obtained without considering the horizontal resistance at the plate bottom (in other words, the stress ratios are close to 100%). However, the differences in the maximum compressive stresses occurred at the plate bottom obtained with and without considering the horizontal resistance are larger with the model developed using the shell elements.

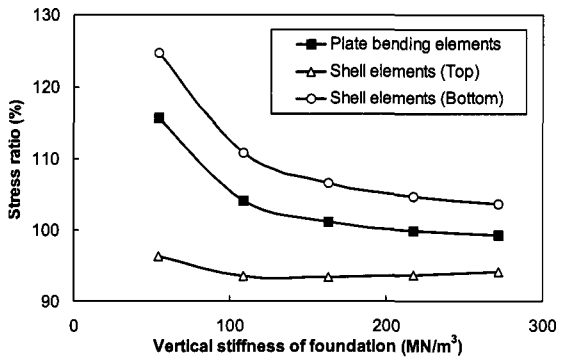

Fig. 9 Comparison of effects of horizontal resistance at plate bottom between plates with and without considering in plane deformations with temperature gradient.

9. Horizontal Resistance Effects with Uniform Temperature Drop

The effect of the horizontal resistance at the plate bottom on the stresses when the uniform temperature drop occurs throughout the plate is investigated. Fig. 10 shows the maximum stresses at the top and bottom of the plate for different values of the horizontal resistance at the plate bottom. As expected, the tensile stresses at both the top and bottom of the plate increase as the horizontal stiffness value increases. There are large differences between the stresses at the top and bottom of the plate even with a small value of the horizontal resistance.

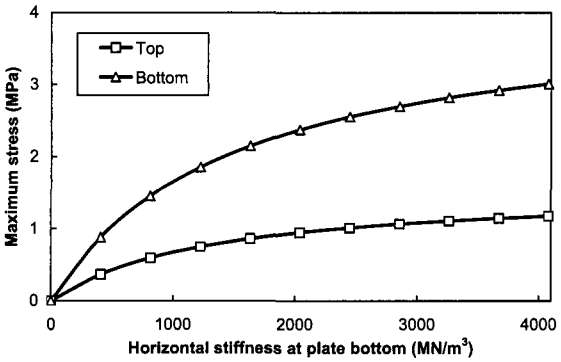

Fig. 10 Effect of horizontal resistance at plate bottom on stresses with uniform temperature drop.

The effects of the variables on the stresses at the top and bottom of the plate when the plate is subjected to the uniform temperature drop with the horizontal stiffness per unit area of 1,632MN/m^3(6,000pci) are shown in Fig. 11. As the thickness of the plate increases, the maximum tensile stresses at the top and bottom of the plate decrease as shown in Fig. 11(a). The stress decrease at the plate bottom is slight, but that at the plate top is rapid as the plate thickness increases. The effect of the vertical stiffness of the foundation is shown in Fig. 11(b). As the vertical stiffness of the foundation increases, the maximum tensile stress at the plate bottom decreases slightly but the tensile stress at the top of the plate increases. Accordingly, the difference

in the stresses at the top and bottom of the plate becomes smaller as the vertical stiffness of the foundation increases. Fig. 11(c) shows the effect of the elastic modulus of the plate on the maximum stresses. The maximum tensile stress at the plate bottom increases with increasing the elastic modulus of the plate. The tensile stress at the top of the plate, on the other hand, increases slightly until the elastic modulus becomes close to 17GPa and then decreases as the elastic modulus increases. Therefore, the differences in the stresses at the top and bottom of the plate become larger as the plate thickness and the elastic modulus of the plate increase and the vertical stiffness of the foundation decreases.

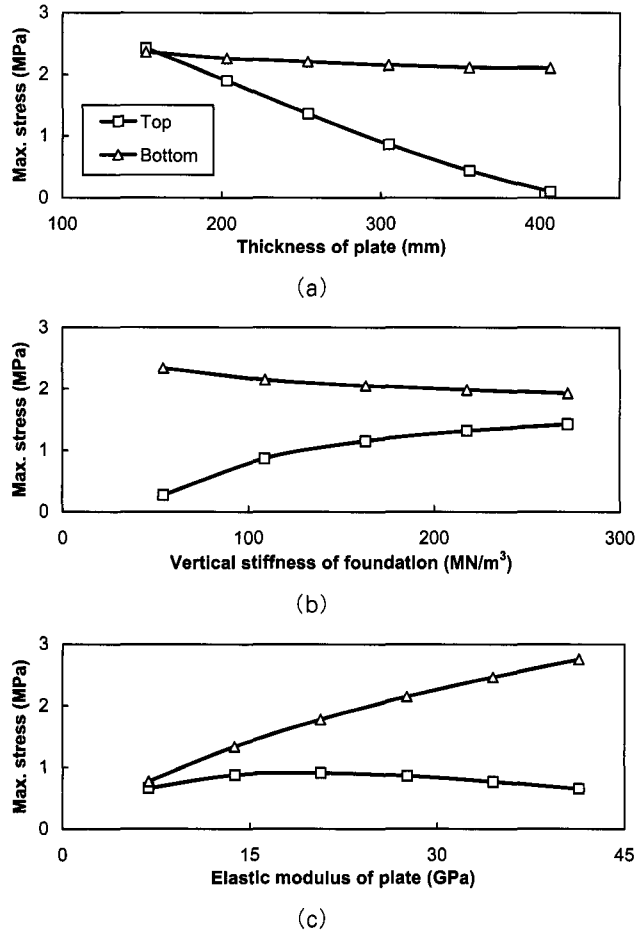

Fig. 11 Stresses at top and bottom of plate when applying a uniform temperature drop for various values of: (a) plate thickness, (b) vertical stiffness of foundation, (c) plate elastic modulus.

10. Summary and Conclusions

The behavior of the concrete slabs on grade considering the horizontal resistance at the slab bottom has been investigated employing the thin plate on a Winkler foundation when the system is subjected to the temperature gradient and uniform temperature drop. Formulations have been developed analytically and numerically to include the effect of the horizontal resistance at the plate bottom. The sensitivity of the horizontal resistance to the stresses of the plate has been investigated with several material and geometric variables. The findings from this study are summarized as follows:

- By incorporating the internal horizontal forces occurred at the plate bottom caused by the horizontal resistance into the equilibrium equations, the governing differential equation that include the horizontal resistance at the plate bottom can be obtained.
- The horizontal resistance effect can be considered in the finite element analysis with the plate bending elements and the flat shell elements without increasing the number of degrees of freedom.
- When the plate is subjected to a temperature gradient, the effect of the horizontal resistance at the plate bottom on the maximum stress becomes significant as the plate thickness and the elastic modulus of the plate increase and the vertical stiffness of the foundation decreases.
- If the in plane horizontal deformations are considered, the location of the neutral surface changes from the middle surface of the plate due to the horizontal resistance at the plate bottom. As a result, the magnitudes of the stresses at the top and bottom of the plate are different; one increases and the other decreases.
- When the plate is subjected to a uniform temperature drop, the differences in the stresses at the top and bottom of the plate, which occur due to the horizontal resistance at the plate

bottom, become larger as the plate thickness and the elastic modulus of the plate increase and the vertical stiffness of the foundation decreases.

The analysis results obtained with the finite element model developed using the shell elements are basically the same as those obtained with the model developed using the 3D solid elements when the horizontal resistance at the plate bottom is considered. Since the model consisting of the shell elements needs much smaller computation time and memory compared with the 3D analysis, it is very useful for practical purposes.

References

ABAQUS. (1998), *User's Manual Version 5.8*, Hibbit, Karlsson & Sorensen, Inc.

Huang, M. H., Thambiratnam, D. P. (2001), Deflection Response of Plate on Winkler Foundation to Moving Accelerated Loads, *Engineering Structures*, 23(9), pp.1134~1141.

Huang, Y. H. (1993), Pavement Analysis and Design, *Prentice Hall*, New Jersey, p.792.

Kim, S. M., Nam, J. H., McCullough, B. F. (2003), Sensitivity of Design Variables to Continuously Reinforced Concrete Pavement Behavior, *Proceedings of the 82nd Annual Meeting of Transportation Research Board*, National Research Council, Washington, D.C. (CD ROM).

Kim, S. M., Roesset, J. M. (1997), Dynamic Response of Pavement Systems to Moving Loads, *Geotechnical Engineering Report GR97-4*, Geotechnical Engineering Center, The University of Texas at Austin.

Kim, S. M., Roesset, J. M. (1998), Moving Loads on a Plate on Elastic Foundation, *ASCE Journal of Engineering Mechanics*, 124(9), pp. 1010~1016.

Kim, S. M., Won, M. C., McCullough, B. F. (2002), Dynamic Stress Response of Concrete Pavements to Moving Tandem Axle Loads, Transportation Research Record, *Journal of the Transportation Research Board*, 1809, pp. 32~41.

Kim, S. M., Won, M. C., McCullough, B. F. (2000), Three Dimensional Analysis of Continuously Reinforced Concrete Pavements, Transportation Research Record, *Journal of the Transportation Research Board*, 1730, pp. 43~52.

Liu, C., McCullough, B. F., Oey, H. S. (2000), Response of Rigid Pavements Due to Vehicle Road Interaction, *ASCE Journal of Transportation Engineering*, 126(3), pp.237~242.

Szilard, R. (2004), Theories and Applications of Plate Analysis, *John Wiley & Sons Inc.*, p. 1056.

Tabatabaie, A. M., Barenberg, E. J. (1980), Structural Analysis of Concrete Pavement Systems, *ASCE Transportation Engineering Journal*, 106(5), pp.493~506.

Westergaard, H. M. (1925), Stresses in Concrete Pavements Computed by Theoretical Analysis, *Public Roads*, 7, pp.25~35.